Full Paper

A New Enzyme Immobilization Technique Based on Thionine-Bovine Serum Albumin Conjugate and Gold Colloidal Nanoparticles for Reagentless Amperometric Biosensor Applications

Shihong Chen, *Ruo Yuan*,* *Yaqin Chai*, *Na Li*

Chongqing Key Laboratory of Analytical Chemistry, College of Chemistry and Chemical Engineering, Southwest University, Chongqing 400715, P. R. China
*e-mail: yuanruo@swu.edu.cn

Received: August 3, 2007
Accepted: October 30, 2007

Abstract
A novel enzyme immobilization technique based on thionine-bovine serum albumin conjugate (Th-BSA) and gold colloidal nanoparticles (nano-Au) was developed. Thionine was covalently bound onto the BSA film with glutaraldehyde(GA) as cross-linker to achieve Th-BSA conjugate. The free amino groups of thionine were then used to attach nano-Au for the immobilization of horseradish peroxidase (HRP). Such nano-Au/Th-BSA matrix shows a favorable microenvironment for retaining the native activity of the immobilized HRP and thionine immobilized in this way can effectively shuttle electrons between the electrode and the enzyme. The proposed biosensor displays excellent catalytic activity and rapid response for H_2O_2. The linear range for the determination of H_2O_2 is from 4.9×10^{-7} to 1.6×10^{-3} M with a detection limit of 2.1×10^{-7} M at 3σ and a Michaelies-Menten constant K_M^{app} value of 0.023 mM.

Keywords: Thionine-bovine serum albumin conjugate, Gold colloidal nanoparticles, Horseradish peroxidase, Hydrogen peroxide, Biosensors

DOI: 10.1002/elan.200704072

1. Introduction

Since the1990s, amperometric enzyme-based biosensors have been an active research field for their potential application to a wide range of analytical tasks, such as clinical diagnosis, environmental monitoring and bioassay [1, 2]. Electron transfer between an electrode and the redox activity center of an enzyme is the basis for developing various enzyme-based biosensors. It can be achieved through two different pathways. One involves direct electron transfer between redox proteins and the electrode. Many materials, such as surfactants [3], polymers [4], inorganic nanomaterials [5] and carbon nanotubes [6, 7] have been reported to realize the direct electron transfer of redox proteins. However, the sensitivity and the application of these unmediated sensors are limited due to the slow electron transfer rate as result of the fact that the redox centers of most enzymes are deeply buried inside insulated protein shells. The other pathway involves electron-shuttling mediators such as hexacyanoferrates [8], ferrocene and its derivatives [9, 10], tetrathiafulvalene [11], quinine [12] and redox dyes [13–16] to establish an electrical communication between redox proteins and the underlying electrodes. In general, mediated enzyme-based biosensors display high sensitivity and low detect limit. Therefore, mediator-based enzyme techniques are the most hopeful for practical uses and investigation of new strategies for preparing the mediated biosensors is a prevailing subject in the design of sensors at present.

A variety of approaches and strategies have been used to immobilize mediators, including electropolymerization [13], adsorption [17, 18], entrapment [15], and covalent linking [16, 19–21]. Nevertheless, there are still several challenges concerning immobilization of electron-shuttling mediators on the electrode surface since low molecular weight soluble mediators can easily diffuse away from the electrode surface into the bulk solution when the biosensor is used continuously, which would lead to significant signal loss and greatly affect the performance and lifetime of the biosensor. Such limitation could be overcome by covalent linking methods, which commonly involve two cases. One is to bind covalently a mediator to a precursor molecule which has been immobilized on the electrode surface using a bifunctional reagent such as glutaraldehyde and terephthaloyl chloride. Deng et al. developed H_2O_2 biosensors based on thionine monolayer which was covalently bound onto a self-assembled cysteamine monolayer [16] and thionine multilayer which were covalently tethered to the multilayer HRP [21], respectively. In these schemes, however, cross-linking with glutaraldehyde was used for enzyme immobi-

lization in the preparation of biosensors, which might denature enzyme and thus lead to low sensitivity and short lifetime of biosensors. In addition, a NADH sensor [22] and a CEA immunosensor [23] were reported by covalently binding thionine to a cysteamine self-assembled monolayer with terephthaloyl chloride as a linkage. The other case is to attach covalently mediators such as phenothiazine derivatives onto a chitosan (CHIT) chains [14, 19, 20] or ferrocene derivatives onto flexible dendritic macromolecules [24], polymer backbones [25], active proteins [26] or inert proteins [27] and then such mediator conjugates are deposited on the surface of electrodes or incorporated into the carbon paste electrodes to achieve the immobilization of mediators. For instance, Ju et al. [28] reported a H_2O_2 sensor based on ferrocene-bovine serum albumin and multiwall carbon nanotubes. Gorski group reported NADH biosensors based on CHIT-TOB/CNT [19] and CHIT-AZU/CNT composite [20], respectively. Due to the increase of the molecular weight of mediators, the leakage significantly decreases. Whereas, these systems usually could not avoid excessively laborious organics synthesis work.

In previous works, we used Nafion [29], L-cysteine/nano-Au film [30] and BSA-HRP composite [31] as entrapping matrix of thionine, toluidine blue and tris(2,2′-bipyridyl)cobalt(III), respectively, to construct mediator-based biosensors. In this work, bovine serum albumin (BSA), an inert protein with rich amino groups (lysine) was chosen as a matrix to covalently bind thionine using glutaraldehyde as cross-linker to achieve Th-BSA conjugate. Nano-Au, as an immobilizing matrix of enzyme, with remarkable features and properties such as large surface area, high-surface free energy, favorable microenviment for retaining biological activity of enzymes and the ability to transfer the electron between enzyme and the electrode, was then attached to Th-BSA through strong binding interactions between nano-Au and the free amino groups of thionine. Finally, horseradish peroxidase (HRP), selected as a model enzyme, was immobilized onto this resulting nano-Au/Th-BSA composite to obtain a H_2O_2 biosensor. To our knowledge, up to now, similar construction strategy has not been reported. The combination of the electron-shuttling property of Th-BSA conjugate with remarkable features and properties of nano-Au provides a new and promising platform for mediator-based electrochemical devices.

2. Experimental

2.1. Reagents

Horseradish peroxidase (HRP) (250 U/mg) and thionine (Th) was obtained from the Shanghai Biochemical Co., China. Bovine serum albumin (BSA), gold chloride tetrahydrate and sodium citrate were purchased from Sigma. Hydrogen peroxide (H_2O_2, 30% w/v solution) and glutaraldehyde were obtained from Chemical Reagent Co., Chongqing, China. The diluted H_2O_2 solutions were prepared from 30% H_2O_2 and the concentration was determined by titration with potassium permanganate. Phosphate buffer solutions (PBS) were prepared with stock standard solutions of 0.1 M KH_2PO_4 and 0.1 M Na_2HPO_4. The supporting electrolyte was 0.1 M KCl. All other chemicals were of reagent grade and used as received, twice-distilled water was used throughout. A stock solution of 1 mg/mL HRP was freshly prepared with 0.1 M PBS (pH 6.0). Gold colloidal nanoparticles with mean size of 16 nm were produced by reducing gold chloride tetrahydrate with sodium citrate at 100 °C for half an hour [32].

2.2. Apparatus and Measurements

Amperometric experiments and cyclic voltammetric experiments were performed using a CHI 660A electrochemical work station (Shanghai CH Instruments Co., China). A three-electrode electrochemical cell consisted of a modified gold electrode as working electrode, a platinum wire as auxiliary electrode, and a saturated calomel electrode (SCE) as reference electrode was employed. All potentials were measured and reported versus the SCE. The test solutions were 5 ml PBS, which were deoxygenated with highly pure nitrogen for 10 min before electrochemical experiments and a nitrogen atmosphere was kept over the solution during measurements. Electrochemical impedance spectroscopy (EIS) measurements were done with a Model IM6e (ZAHNER Elektrick Co., Germany) in the presence of a 5.0 mM $K_3[Fe(CN)_6]$ /$K_4[Fe(CN)_6]$ (1:1) mixture as a redox probe. All the electrochemical experiments were carried out at room temperament.

Atomic force microscopy (AFM) images of the films were achieved by scanning probe microscope (SPM) (Vecco, USA). X-ray photoelectron spectroscopy (XPS) measurements were performed on a VG Scientific ESCALAB 250 spectrometer, using Al Kα X-ray (1486.6 eV) as the light source. Infrared spectra (IR) were collected with a Fourier-transform infrared spectrophotometer (GX, Perkin Elmer Co., USA) using KBr disks. The size of gold colloidal nanoparticles was estimated from transmission electron microscopy (TEM) (TECNAI 10, PHILIPS FEI Co., Holland).

2.3. Preparation of Hydrogen Peroxide Biosensor

The gold electrode (4 mm diameter) was carefully polished with 1.0 and 0.3 μm alumina slurries to obtain mirror like surface. After rinsing with water, the polished electrode was immersed in freshly prepared 3:7 mixtures of 30% hydrogen peroxide and concentrated sulfuric acid for 10 minutes and then rinsed thoroughly with water, followed by cleaning with acetone and twice-distilled water in an ultrasonic bath, respectively. Allowed to dry at room temperature, the electrode was immediately coated with 15 μL 50 mg/mL BSA solution (prepared in 0.1 M pH 7.0 PBS) and left for 24 h at 4 °C in a refrigerator to allow the BSA film to dry. Then, the BSA modified electrode was immersed into 2.5%

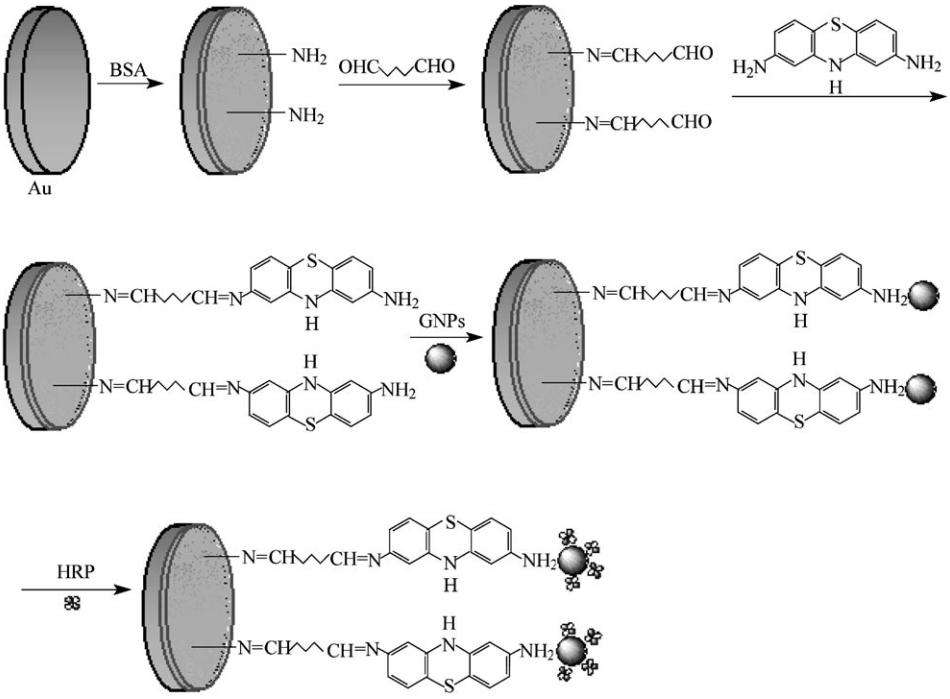

Scheme 1. Illustration of the preparation process of hydrogen peroxide biosensor.

glutaraldehyde for 20 min and washed with water. Later, the electrode was incubated in aqueous solution containing 1.0×10^{-3} M thionine for 12 h, followed by drying in a refrigerator (4 °C) to produce stable Th-BSA film modified electrode. After thoroughly rinsed with twice-distilled water and PBS (pH 7.0), it was immersed in gold colloid solution for 8 h to achieve nano-Au/Th-BSA matrix modified electrode. Finally, it was incubated in HRP solution overnight. The resulting electrode, denoted as HRP/nano-Au/Th-BSA/Au, was stored in a refrigerator (4 °C) until further use. The preparation process of the biosensor is shown in scheme 1.

3. Results and Discussion

3.1. Atomic Force Microscopy (AFM)

The surface morphology of the enzyme films was observed with AFM. Figure 1 illustrates the typical AFM images (including height figure and phase figure) of the bare gold substrate, BSA, nano-Au/Th-BSA and HRP/nano-Au/Th-BSA films modified gold surface, respectively. By comparing the AFM image of the bare gold substrate (Fig. 1a) with that of BSA film (Fig. 1b), it can be seen that BSA was successful cast on the gold substrate surface and formed a porous hydrogel. After thionine and nano-Au were successively grafted onto BSA, many globular particles are observed at the AFM image of the resulting film (Fig. 1c), which is ascribed to the assembly of nano-Au. The phase figure part in the AFM image of HRP/nano/Th-BSA films (Fig. 1d) exhibits a smoothing effect as compared to that of nano/Th-BSA films, which might be due to HRP molecules filling the interstitial places between nano-Au particles.

3.2. X-Ray Photoelectron Spectroscopy (XPS)

To gain information concerning the formation of Th-BSA conjugate and the adsorption of nano-Au onto Th-BSA, XPS measurements were performed. Figure 2A curve a is the C1s XPS spectra for the composites of BSA and glutaraldehyde (GA), denoted GA-BSA. It can be noted that there are three intense C1s peaks centered at 295.0 eV, 292.4 eV and 284.0 eV, respectively. When thionine was grafted onto the GA-BSA (Fig. 2A, curve b), the high binding energy C 1s peaks at 295.0 eV and 292.4 eV detected on GA-BSA composites almost completely disappear, which may provide evidence for the formation of the Th-BSA conjugate by the interaction between BSA and thionine with glutaraldehyde as cross-linker. After nano-Au was absorbed onto Th-BSA conjugate, the Au4f XPS measurement was carried out to confirm the presence of Au metal. As expected, Au4f doublet features with binding energies of 83.5 eV for $4f_{7/2}$ and 87.2 eV for $4f_{5/2}$ can be clearly observed at the nano-Au/Th-BSA composites (Fig. 2B), indicating that gold colloidal nanoparticles are indeed successfully attached onto the Th-BSA conjugate.

3.3. Infrared Spectra (IR)

In order to further gain information concerning the modification reaction between thionine and BSA and

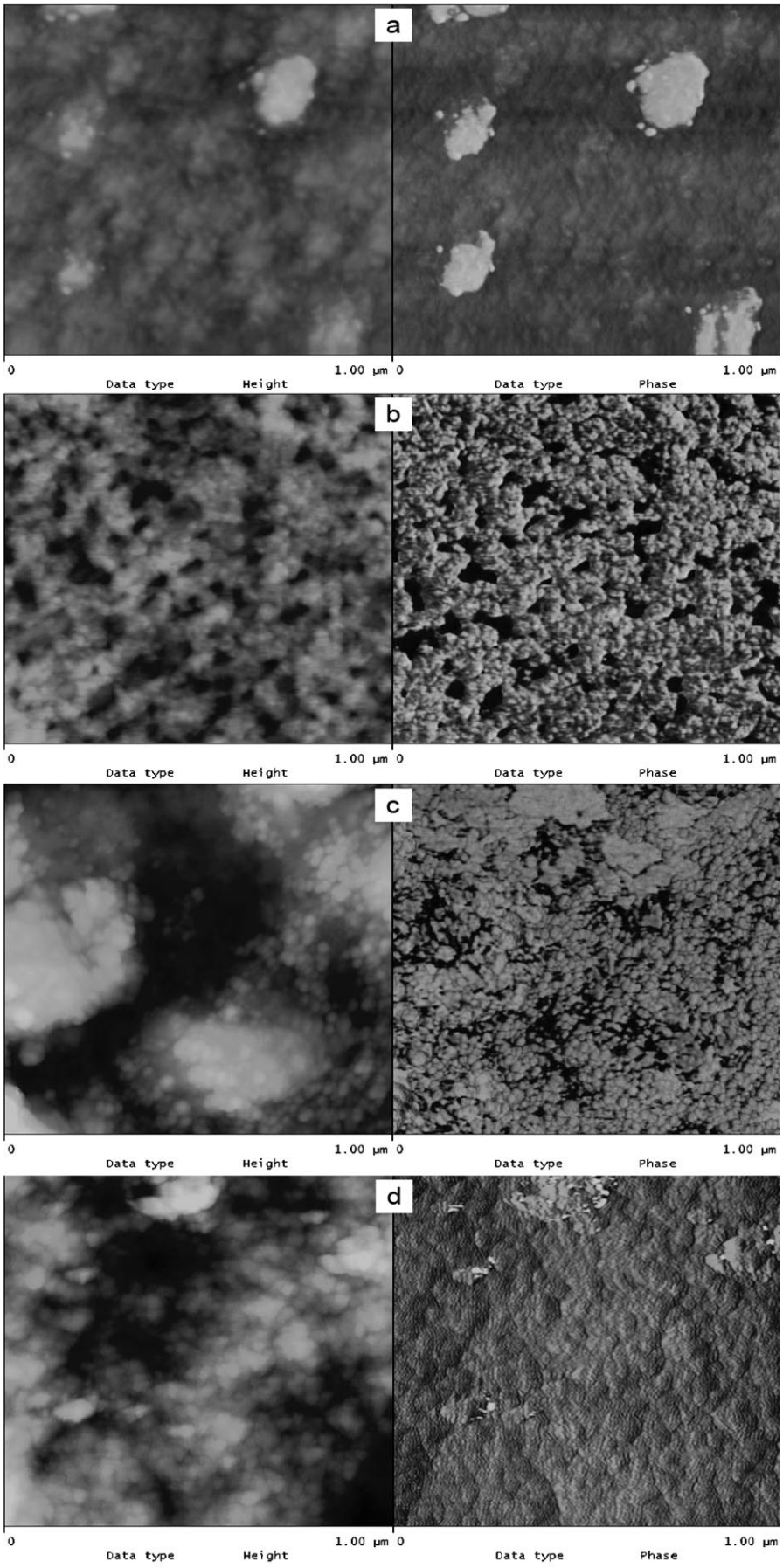

Fig. 1. AFM images of a) bare gold substrate, b) BSA film, c) nano-Au/Th-BSA film and d) HRP/nano-Au/Th-BSA film on the gold surface.

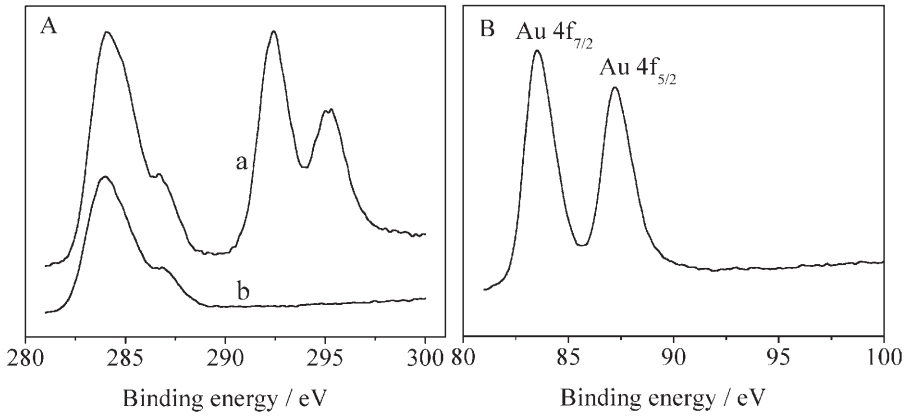

Fig. 2. A) C1s XPS spectra of a) GA-BSA composites and b) Th-BSA composites. B) Au4f XPS spectra of nano-Au/Th-BSA composites.

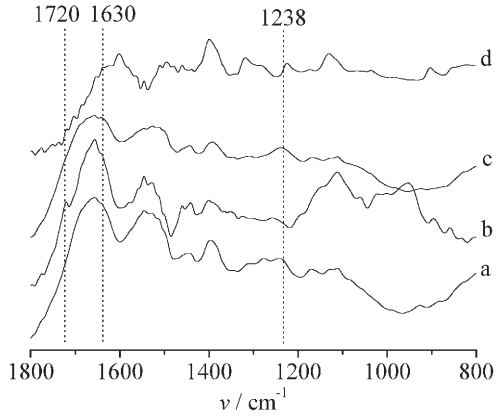

Fig. 3. Infrared spectra of a) BSA, b) GA-BSA, c) Th-BSA, and d) thionine.

determine the extent of aldehyde groups' utilization in the cross-linking process, the IR spectra measurements were performed on BSA, GA-BSA composites, Th-BSA conjugate and thionine, respectively. The results are shown in Figure 3. In contrast to the BSA sample (curve a), GA-BSA composites (curve b) present a characteristic adsorption band at 1720 cm^{-1}, which is due to the free aldehyde group. This confirms that glutaraldehyde molecules are grafted onto BSA by one end, leaving a free aldehyde group on the other end. After GA-BSA composites reacted with thionine, in the spectrum of resulting composites Th-BSA (curve c), the disappearance of the adsorption band at 1720 cm^{-1} and the appearance of adsorption band at 1630 cm^{-1} and 1238 cm^{-1}, which could be ascribed to absorption by aromatic rings of thionine (curve d), confirm that thionine molecules could be covalently grafted onto GA-BSA composites based on the reaction between the free aldehyde groups of GA-BSA and the amino groups of thionine to form Schiff bases.

3.4. Electrochemical Impedance Spectroscopy (EIS)

EIS was used to characterize the stepwise assembly of the hydrogen peroxide biosensor. The linear part, observed in the EIS, represents the diffusion-limited process. The semicircle portion in the EIS corresponds to the electron-transfer-limited process and the semicircle diameter equals the electron-transfer resistance (R_{et}). Figure 4 displays the EIS on different modified electrodes in presence of redox probe $Fe(CN)_6^{4-/3-}$. As can be seen, the EIS of bare gold electrode is almost a straight line (curve a), implying very low R_{et} on bare gold electrode to the redox probe dissolved in the electrolyte solution. The EIS of BSA coated electrode shows a high interfacial R_{et} ($R_{et} = 1710\ \Omega$, curve b), indicating that the insulating BSA membrane obstructs the electron transfer of the electrochemical probe. After thionine was covalently bound onto the BSA film, the R_{et} decreases to 507 Ω (curve c), which proves that, thionine, as electron-shuttling mediator, is beneficial to the electron transfer. When nano-Au was adsorbed onto Th-BSA film, a further decrease of R_{et} is observed (curve d), which is attributed to the good conductive properties of nano-Au. Compared with the nano-Au/Th-BSA modified electrode, the EIS of HRP/nano-Au/Th-BSA modified electrode presents an obvious increase in R_{et} ($R_{et} = 875\ \Omega$, curve e). This increase is due to the non-conductive properties of HRP. The impedance change obtained after the modification process proves that BSA, thionine, nano-Au and HRP have been successively assembled on the gold electrode.

3.5. Electrochemical Characteristics of Hydrogen Peroxide Biosensor

The cyclic voltammograms (CVs) of the biosensor, namely HRP/nano-Au/Th-BSA/Au electrode, give a pair of well-defined redox peaks in PBS (pH 6.5) at scan rate of 50 mV/s (Fig. 5, curve a), characteristic of redox couple of thionine. Anodic and cathodic peak potentials are at −145 mV and −195 mV, respectively. The peak-to-peak separation is

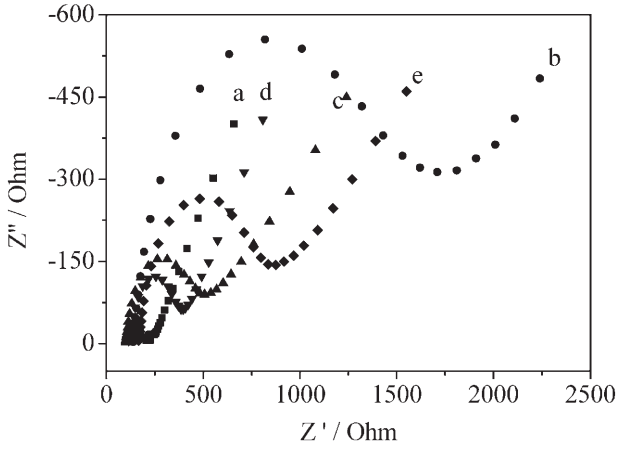

Fig. 4. EIS of bare Au (a), BSA/Au (b), Th-BSA/Au (c), nano-Au/Th-BSA/Au (d), and HRP/nano-Au/Th-BSA/Au (e) electrodes in 5.0 mM $K_3Fe(CN)_6$/ $K_4Fe(CN)_6$ (1:1).

50 mV at scan rate of 50 mV/s, indicative of facile charge transfer kinetics. The CVs at different scan rates show that both anodic and cathodic peak currents increase linearly with the square root of scan rate between 10 and 120 mV/s (data not shown), indicating that the reduction and oxidation of the TH/TH^+ couple is diffusion-controlled at the modified electrode.

The catalytic activity of the biosensor toward H_2O_2 was investigated by cyclic voltammetry. Figure 5 illustrates the CVs recorded for the biosensor in PBS (pH 6.5) containing varied concentration of H_2O_2. In the meantime, a control experiment was performed at nano-Au/Th-BSA/Au electrode (data not shown). It is found that this modified electrode without HRP doesn't exhibit catalytic activity for the reduction of H_2O_2. Whereas, the catalytic reduction of H_2O_2 at HRP/nano-Au/Th-BSA/Au electrode can be seen clearly in Figure 5. With the addition of H_2O_2, reduction peak current increased significantly while oxidation peak current decreased, indicating that a catalytic reaction

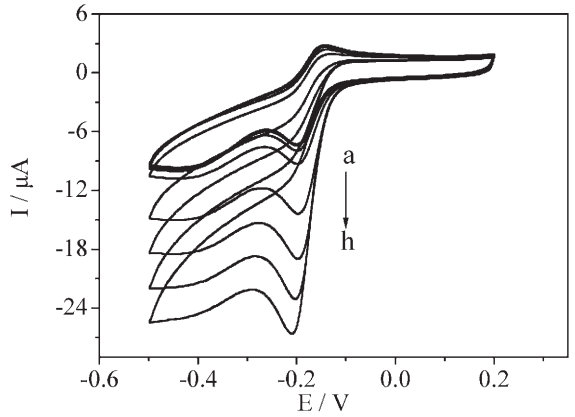

Fig. 5. CVs of the biosensor in 0.1 M PBS (pH 6.5) without H_2O_2 (a), with 0.113 mM (b), 0.182 mM (c), 0.298 mM (d), 0.682 mM (e), 1.03 mM (f), 1.31 mM (g), and 1.63 mM (h) H_2O_2. Scan rate: 50 mV/s.

occurred on this biosensor. These results demonstrate that the response of the biosensor to H_2O_2 results from only the catalytic activity of HRP immobilized onto nano-Au/Th-BSA matrix and thionine incorporated in Th-BSA conjugate can effectively shuttle electrons between the base electrode and the redox activity center of HRP. The reduction of H_2O_2 catalyzed by HRP and mediated by thionine can be described as follow.

Firstly, H_2O_2 is reduced by immobilized $HRP_{(Red)}$:

$$H_2O_2 + HRP_{(Red)} \rightarrow HRP_{(Ox)} + H_2O$$

Then the $HRP_{(Ox)}$ produced in enzymatic reaction oxidizes the reduced form of thionine (TH) to the oxidized form (TH^+),

$$HRP_{(Ox)} + TH \rightarrow HRP_{(Red)} + TH^+$$

Finally, the TH^+ formed is electrochemically reduced at the electrode and recycles, leading to a reduction current:

$$TH^+ + H^+ + 2e \rightarrow TH_2$$ [33]

3.6. Optimum of Analytical Condition

The pH value is one of the parameters which affect the catalytical reduction of H_2O_2 on the biosensor. The change of chronoamperometric current with the pH under constant H_2O_2 concentration (2.8×10^{-4} M) was studied. The results show that the maximum response appears at pH 6.5 (not shown here). So pH 6.5 phosphate buffer solutions were selected for the determination of H_2O_2.

The effect of applied potential on the response of the biosensor toward constant concentration (2.8×10^{-4} M) H_2O_2 was also investigated. The results show that the response current gradually increases with decreasing negatively applied voltage from 0 to -400 mV (not shown here). Although a more negatively applied voltage would lead to a higher sensitivity, it is preferable to control a more positively applied voltage in order to avoid or decrease the interference caused by some electroactive species [17]. Hence, a working potential of -200 mV was chosen for H_2O_2 determination in this work, where the sensor could maintain reasonable sensitivity and avoid the interference caused by some electroactive species.

3.7. Response of the Biosensor to Hydrogen Peroxide

Figure 6 pictures the chronoamperometric response of the biosensor to different concentration of H_2O_2 under the optimized conditions. It can be observed that increasing the concentration of H_2O_2 added into the solution results in an apparent increase in the reduction current. Moreover, the biosensor achieves 95% of the steady-state current in less than 10 s, indicating a fast response process. The inset of Figure 6 displays the calibration curve of the biosensor for

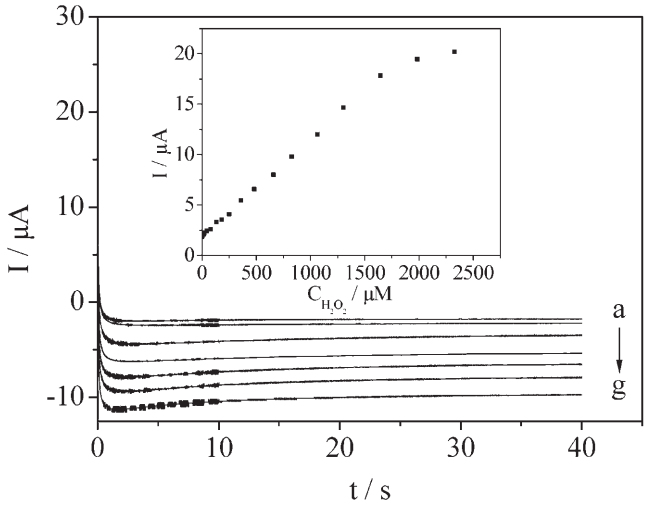

Fig. 6. Amperometric response of the biosensor in a pH 6.5 PBS containing 0, 0.025, 0.18, 0.36, 0.48, 0.66 and 0.83 mM H_2O_2 (from a to g) at an applied potential of −200 mV. Inset shows linear calibration curves.

H_2O_2 determination. The linear range spans the concentration of H_2O_2 from 4.9×10^{-7} to 1.6×10^{-3} M. The linear regression equation is i (μA) = 1.88 + 9.6 [H_2O_2] (mM) with a correlation coefficient of 0.998 ($n = 19$). From the slope of calibration curve, the detection limit of 2.1×10^{-7} M is estimated at signal-to-noise ration of three. When the concentration of H_2O_2 is higher than 1.6×10^{-3} M, a response plateau appears, showing the characteristics of the Michaelis–Menten kinetic mechanism. The apparent Michaelis–Menten constant (K_M^{app}) is calculated to be 0.023 mM according to the Lineweaver–Burk equation [34]. This value is 1217 times smaller than 28 mM for the H_2O_2 biosensor based on the entrapment of HRP into poly(thionine) film [35], 70 times smaller than 1.6 mM for the H_2O_2 biosensor based on the coimmobilization of HRP and thionine using glutaraldehyde on the electrode [36]. The low value of K_M^{app} means that HRP immobilized on the nano-Au/Th-BSA matrix retains well its bioactivity and has a high affinity to H_2O_2.

3.8. Reproducibility, Stability, and Interference of the Hydrogen Peroxide Biosensor

The biosensor shows good reproducibility for the determination of H_2O_2 concentration in its linear range. The relative standard deviation (*RSD*) is 2.8% for twelve successive assays at the H_2O_2 concentration of 0.10 mM.

The storage stability of the proposed biosensor was also studied. When the electrode was kept by suspending it above 0.1 M PBS (pH 6.5) at 4 °C in a refrigerator, the current response to 0.10 mM H_2O_2 decreased 3.5% of its initial value after 3 days, 9.8% for two weeks and 21% for 1 month, showing a longer lifetime.

The potential interference of some biological substance was investigated. The interference degree from interfering substances can be evaluated by virtue of the current ratio values, which were calculated by comparing the current of the proposed biosensor in an assay solution containing both 0.020 mM H_2O_2 and a 0.10 mM interfering substance with that of the proposed biosensor in an assay solution containing only 0.020 mM H_2O_2. They are 1.06 for glucose, 1.06 for ascorbic acid, 1.01 for uric acid, 0.97 for L-cysteine and 1.02 for L-tyrosine. These results indicate that above five tested interferents would not cause observable interference to the determination of H_2O_2. In addition, oxygen displayed an obvious interference. Hence, in our experiments, the test solutions were deaerated by high pure nitrogen, and a nitrogen atmosphere was kept over the solution during measurements to avoid the interference of oxygen.

Table 1. The recoveries of H_2O_2 tested with hydrogen peroxide biosensor.

Added H_2O_2 (mM)	Found H_2O_2 (mM)		
	Mean ± *SD*	*RSD* (%)	Recovery (%) [a]
0.080	0.075 ± 0.004	5.3	93.8
0.150	0.148 ± 0.010	6.8	98.7
0.650	0.625 ± 0.022	3.5	96.2
1.20	1.24 ± 0.08	6.5	103

[a] Calculated as a mean of three measurements.

3.9. Recovery Experiment

The analytical applicability of the biosensor was evaluated by determining the recoveries of different concentration H_2O_2 by a calibration curve method. The results were listed in Table 1. The biosensor shows satisfactory results, with the recovery rate in the range 93.8% – 103%.

4. Conclusions

A new strategy was proposed to immobilize enzyme for the fabrication of reagentless amperometric biosensor. First, thionine was covalently bound onto the BSA film to obtain Th-BSA conjugate. Then, nano-Au was adsorbed onto it to achieve nano-Au/Th-BSA matrix for the immobilization of HRP. The resulting system provides a new biocomposite platform for electrochemical devices. Immobilized HRP possesses high enzymatic activity and high affinity for H_2O_2, characterized by low apparent Michaelis–Menten constant, broad linear range and low detection limit for H_2O_2 determination.

5. Acknowledgements

This work was financially supported by the National Natural Science Foundation of China (NO. 20675064), the Natural Science Foundation of Chongqing City (NO. CSTC-

2004BB4149, 2005BB4100) and High Technology Project Foundation of Southwest University (XSGX 02).

6. References

[1] P. D. Hale, L. I. Boguslavsky, T. Inagaki, H. I. Karan, H. S. Lee, T. A. Skotheim, *Anal. Chem.* **1991**, *63*, 677.
[2] J. Li, L. T. Xiao, X. M. Liu, G. M. Zeng, G. H. Huang, G. L. Shen, R. Q. Yu, *Anal. Bioanal. Chem.* **2003**, *376*, 902.
[3] J. F. Rusling, A. E. F. Nassar, *J. Am. Chem. Soc.* **1993**, *115*, 11891.
[4] A. E. F. Nassar, J. F. Rusling, *J. Am. Chem. Soc.* **1996**, *118*, 3043.
[5] K. R. Brown, A. P. Fox, M. J. Natan, *J. Am. Chem. Soc.* **1996**, *118*, 1154.
[6] J. X. Wang, M. X. Li, Z. J. Shi, N. Q. Li, Z. N. Gu, *Anal. Chem.* **2002**, *74*, 1993.
[7] S. H. Chen, R. Yuan, Y. Q. Chai, L. Y. Zhang, N. Wang, X. L. Li, *Biosens. Bioelectron.* **2007**, *22*, 1268.
[8] F. Schubert, S. Saini, A. P. F. Turner, *Anal. Chim. Acta* **1991**, *245*, 133.
[9] T. Tatsuma, Y. Okawa, T. Watanabe, *Anal. Chem.* **1989**, *61*, 2352.
[10] A. Mulchandani, C. L. Wang, H. H. Weetall, *Anal. Chem.* **1995**, *67*, 94.
[11] F. Wendzinski, B. Grundig, R. Renneberg, F. Spener, *Biosens. Bioelectron.* **1997**, *12*, 43.
[12] P. D. Sanchez, P. T. Blanco, J. M. F. Alvarez, M. R. Smyth, R. O'Kennedy, *Electroanalysis* **1990**, *2*, 303.
[13] A. A. Karyakin, A. K. Strakhova, E. E. Karyakina, S. D. Varfolomeyev, A. K. Yatsimirsky, *Bioelectrochem. Bioenerg.* **1993**, *32*, 35.
[14] Y. E. Sorunmu, M. Nguyen, J. B. Sapp, W. Gorski, T. D. Phan, X. Wei, *Electroanalysis* **2006**, *18*, 2375.
[15] C. Ramirez Molina, M. Boujtita, N. El Murr, *Anal. Chim. Acta* **1999**, *401*, 155.
[16] C. M. Ruan, R. Yang, X. H. Chen, J. Q. Deng, *J. Electroanal. Chem.* **1998**, *455*, 121.
[17] C. H. Lei, J. Q. Deng, *Anal. Chem.* **1996**, *68*, 3344.
[18] X. Chen, J. Z. Zhang, B. Q. Wang, G. J. Cheng, S. J. Dong, *Anal. Chim. Acta* **2001**, *434*, 255.
[19] M. G. Zhang, W. Gorski, *J. Am. Chem. Soc.* **2005**, *127*, 2058.
[20] M. G. Zhang, W. Gorski, *Anal. Chem.* **2005**, *77*, 3960.
[21] C. M. Ruan, F. Yang, C. H. Lei, J. Q. Deng, *Anal. Chem.* **1998**, *70*, 1721.
[22] H. Y. Chen, D. M. Zhou, J. J. Xu, H. Q. Fang, *J. Electroanal. Chem.* **1997**, *422*, 21.
[23] Z. Dai, J. Chen, F. Yan, H. X. Ju, *Cancer Detect. Prev.* **2005**, *29*, 233.
[24] J. Losada, I. Cuadrado, M. Moran, C. M. Casado, B. Alonso, M. Barranco, *Anal. Chim. Acta* **1997**, *338*, 191.
[25] S. Koide, K. Yokoyama, *J. Electroanal. Chem.* **1999**, *468*, 193.
[26] A. Badia, R. Carlini, A. Fernandez, F. Battaglini, S. R. Mikkelsen, A. M. English, *J. Am. Chem. Soc.* **1993**, *115*, 7053.
[27] C. Padeste, A. Grubelnik, L. Tiefenauer, *Biosens. Bioelectron.* **2003**, *15*, 431.
[28] V. S. Tripathi, V. B. Kandimalla, H. X. Ju, *Biosens. Bioelectron.* **2006**, *21*, 1529.
[29] Y. Zhuo, R. Yuan, Y. Q. Chai, D. P. Tang, Y. Zhang, N. Wang, X. L. Li, Q. Zhu, *Electrochem. Commun.* **2005**, *7*, 355.
[30] S. H. Chen, R. Yuan, Y. Q. Chai, L. Xu, N. Wang, X. N. Li, L. Y. Zhang, *Electroanalysis* **2006**, *18*, 471.
[31] Y. Zhuo, R. Yuan, Y. Q. Chai, A. L. Sun, Y. Zhang, J. Z. Yang, *Biomaterials* **2006**, *27*, 5420.
[32] B. V. Enüstün, J. Turkevich, *J. Am. Chem. Soc.* **1963**, *85*, 3317.
[33] H. Durliat, A. Courteix, M. Comtat, *Bioelectrochem. Bioenerg.* **1989**, *22*, 197.
[34] R. A. Kamin, G. S. Wilson, *Anal. Chem.* **1980**, *52*, 1198.
[35] Y. Xiao, H. X. Ju, H. Y. Chen, *Anal. Chim. Acta* **1999**, *391*, 299.
[36] J. J. Xu, D. M. Zhou, H. Y. Chen, *Electroanalysis* **1998**, *10*, 713.

